Fluorescence Depolarization Studies of Filamentous Actin Analyzed with a Genetic Algorithm

Denys Marushchak,* Staffan Grenklo,† Thomas Johansson,† Roger Karlsson,† and Lennart B.-Å. Johansson*
*Department of Chemistry; Biophysical Chemistry, Umeå University, Umeå, Sweden; and †Department of Cell Biology, Wenner-Gren Institute, Stockholm University, Stockholm, Sweden

ABSTRACT A new method, in which a genetic algorithm was combined with Brownian dynamics and Monte Carlo simulations, was developed to analyze fluorescence depolarization data collected by the time-correlated single photon-counting technique. It was applied to studies of BODIPY-labeled filamentous actin (F-actin). The technique registered the local order and reorienting motions of the fluorophores, which were covalently coupled to cysteine 374 (C374) in actin and interacted by electronic energy migration within the actin polymers. Analyses of F-actin samples composed of different fractions of labeled actin molecules revealed the known helical organization of F-actin, demonstrating the usefulness of this technique for structure determination of complex protein polymers. The distance from the filament axis to the fluorophore was found to be considerably less than expected from the proposed position of C374 at a high filament radius. In addition, polymerization experiments with BODIPY-actin suggest a 25-fold more efficient signal for filament formation than pyrene-actin.

INTRODUCTION

Experimental methods like x-ray diffraction (1,2) and nuclear magnetic resonance (3,4) are of central importance to the determination of macromolecular structures. However, intense work is currently put into the development of complementary methods based on electronic energy transfer and fluorescence. For structure determination of complex macromolecular assemblies, these techniques may become especially important. Most of them are based on irreversible energy transfer from an excited donor to an acceptor molecule (5–8), while electronic energy migration between fluorescent molecules of the same kind, so called donor-donor energy migration (DDEM) or homotransfer (9) is used less frequently. Here we have applied the latter technique to study the structure of filamentous actin (F-actin); an ordered noncovalent polymer, resulting from the spontaneous polymerization of actin molecules in the presence of salt, and characterized by a fast and a slow growing end where actin subunits add and dissociate in a constant flux balanced by a stable concentration of unpolymerized G-actin.

Fluorescence spectroscopic experiments based on electronic energy transfer and DDEM can typically provide distance information in the range of 10–100 Å, making it suitable for distance determinations within protein molecules. However, the requirement of introducing fluorescent probes by covalent coupling to one or more specific amino-acid side chains complicates quantitative interpretations of the data. For monomeric proteins this has been largely overcome by the recent development of an extended Förster theory (10,11), but for protein polymers like F-actin, the analyses are complicated by the large number of fluorophores involved in energy migration. In such cases, the spatial and rotational distributions of the interacting donors must be considered. Recently it was demonstrated that Brownian dynamics (BD) and Monte Carlo (MC) simulations can be applied to quantitatively describe the DDEM between fluorescent groups in a regular polymer structure, where fluorophores had been coupled to the protein monomers before they were allowed to copolymerize with nonlabeled molecules and become randomly distributed into the noncovalent polymer (12). This technique enables the determination of local rotational restrictions and motions of the fluorophore and provides the geometrical parameters needed to characterize the structure of the polymer.

The helically twisted structure of F-actin is of methodological interest in this context since it incorporates special cases of linear and ring-shaped structures (12). The characteristic parameters of the polymer (see Fig. 1) constitute the translational distance (T_z), the rotation (θ) of each neighbor protein molecule, and the radial distance between the helical axis and the position of the donor (T_{xy}). For the proposed structure of F-actin, the position of a subunit is obtained from the coordinates of the preceding one by an axial translation by $T_z = 27.5$ Å, and a rotation by $\theta = 166°$ (13). The distance between the helical axis and the C374 is of particular interest since it can be labeled by a fluorescent group; the distance from the C_∞ axis to the center of mass of the donor group would then correspond to the T_{xy}, which was determined to be 13.5 Å by Moens et al. (14). In our

Submitted March 5, 2007, and accepted for publication July 10, 2007.

Address reprint requests to L. B.-Å. Johannson, E-mail: lennart.johansson@chem.umu.se.

S. Grenklo's present address is Department of Microbiology, Tumor and Cell Biology, Karolinska Institutet, Box 280, S-171 77 Stockholm, Sweden.

Some abbreviations used: C_∞, rotational axis of the helical structure; D, donor of electronic energy; **D**, director frame of the donor; $D(t)$, the observed fluorescence difference curve; f, mole fraction of labeling; R_0, the Förster radius; $r(t)$, the time-resolved fluorescence anisotropy; S_j, second-rank order parameter of the j^{th} fluorophore; TCSPC, time-correlated single-photon counting; χ^2, the statistical test parameter.

Editor: Arthur G. Palmer III.

0006-3495/07/11/3291/09 $2.00

doi: 10.1529/biophysj.107.107920

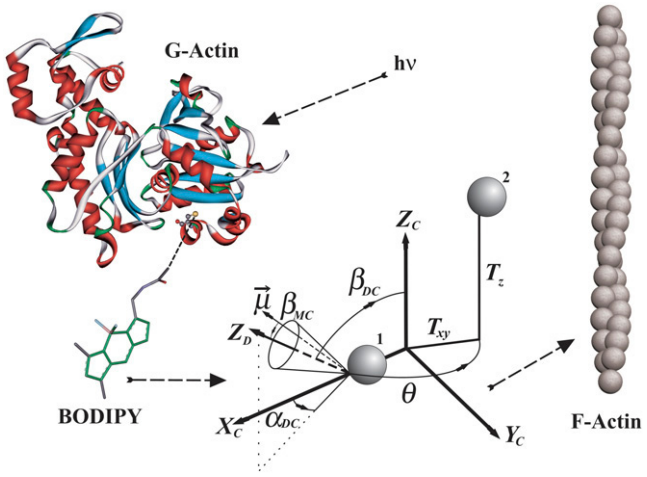

FIGURE 1 The location of C374 targeted with the BODIPY label, and identification of the structural parameters used for assessing the position of this residue in the actin after polymerization. To the left, the molecular structure of G-actin (37,38) is displayed as a ribbon diagram with C374 indicated (*balls* and *sticks*) together with the BODIPY fluorophore. The helical structure to the right represents a hypothetical actin filament. In the center, the parameters, which specify the position of the monomers and the fluorescent group in the polymer are defined. The Z_C axis coincides with the C_∞ axis, and T_{xy} denotes the distance from this axis to the position of a fluorescent group. The translational and the rotational transformations between nearest protein neighbors are T_z and θ, respectively. The fluorophore undergoes local reorienting motions about an effective symmetry axis Z_D, which is transformed to the polymer fixed frame by $\Omega_{DC} = (\alpha_{DC}, \beta_{DC})$.

analysis, we determine a shorter distance, suggesting a closer position of C374 to the filament axis.

METHODS

Preparation of β/γ-actin

β/γ-actin was isolated from calf thymus using poly-L-proline Sepharose and hydroxyl apatite chromatography as described previously (1,2,4). The actin was recovered in 5 mM Tris-HCl, pH 7.6, 0.5 mM ATP, 0.1 mM $CaCl_2$, 0.5 mM DTT (G-buffer) and frozen in 20 μl aliquots added directly into liquid nitrogen. The actin-containing granules were stored in liquid nitrogen.

BODIPY-labeling of β/γ-actin, characterization, and sample preparation

Actin was rapidly thawed, centrifuged at 16,000 $\times$ *g* at 277 K for 20 min, passed through a 0.22 μm filter to remove possible aggregates of denatured protein, and polymerized in the presence of 0.2 mM EGTA by addition of $MgCl_2$ and KCl to 2 and 100 mM, respectively, for 1 h at room temperature before centrifugation at 100,000 $\times$ *g* at 288 K for 1 h. The supernatant was removed, and the pellet washed twice with 20 mM HEPES pH 7.6, containing 0.1 mM $CaCl_2$, 0.1 mM ATP, thoroughly deoxygenated and bubbled with argon before use. After resuspension in the HEPES buffer, the pellet was transferred to an E-flask with a magnetic stir bar and 2 mg *n*-(4,4-difluoro-5,7-dimethyl-4-bora-3a,4a-diaza-*s*-indacene-3-yl)methyl (BODIPY, D-6003; Molecular Probes, Eugene, OR) in 80 μl DMSO was added in 3 μl aliquots. The reaction mixture, protected from light, was left under slow stirring for 1 h at room temperature, followed by homogenization with a Dounce-homogenizer and dialysis against 1 L G-buffer (without DDT) overnight at 277 K (MW cutoff: 12,000–14,000 Da). To ensure complete depolymerization, the homogenization and dialysis procedures were repeated twice except that the G-buffer was supplemented with 0.5 mM DDT. After a final homogenization, the solution was centrifuged at 100,000 $\times$ *g* for 3 h at 277 K to remove residual actin filaments and denatured protein. Protein concentration and BODIPY labeling was determined by absorbance measurements using the extinction coefficients ε_{actin} (290 nm) = 0.63 (mg/ml cm)$^{-1}$, and ε_{BODIPY} (502 nm) = 77,300 (M cm)$^{-1}$ with G-buffer as blank. Labeling efficiency was determined to be 49%, and the location of the BODIPY-group on C374 was assessed by matrix-assisted laser desorption/ionization time-of-flight (MALDI-TOF) by comparing the mass spectrograms of conjugated and nonconjugated actin after sodium dodecyl-sulfate polyacrylamide gel electrophoresis (SDS-PAGE) and in-gel trypsin cleavage as described recently (15).

Polymerization of the actin was recorded using a Fluorskan II plate reader (Labsystems, Vantaa, Finland) equipped with filters for detection of BODIPY and pyrene fluorescence. Actin filaments containing BODIPY-actin were observed with a Leica DMLB epifluorescence microscope, using standard fluorescein excitation/emission filters, a DC350F charge-coupled device camera, and Image Manager 500 software (Leica Microsystems, Wetzlar, Germany); the filaments were stained with TRITC-phalloidin before microscopy.

The fluorescence depolarization experiments were performed with four sample concentrations of BODIPY-labeled actin, 0.1, 12.25, 24.5, and 49%, all having a total actin concentration of 2.4 μM; measurements were performed on both G- and F-actin. For polymerization, the actin-samples in G-buffer containing 0.2 mM EGTA and 0.05% (w/v) NaN_3 were supplemented with $MgCl_2$ and KCl to final concentrations of 2 mM and 100 mM, respectively, and left overnight to reach steady-state polymerization before measurement.

Spectroscopic measurements

Absorption spectra were recorded on a GBC 920 spectrometer (GBC Scientific Equipment, Melbourne, Australia), and fluorescence spectra on a SPEX spectrofluorometer (SPEX Industries, Metuchen, NJ). Both the excitation and emission steady-state anisotropies were monitored for each sample; excitation spectra between 450 and 500 nm, were collected with the emission measured at 515 nm, and emission spectrum measured between 515 and 570 nm, with excitation set to 500 nm. Time-resolved fluorescence experiments were performed on a setup from IBH (Glasgow, Scotland) equipped with a Cyan laser NanoLED-14 (λ = 467 nm), operating at 800 kHz. The excitation and emission wavelengths were selected using monochromators set to 467 and 514 nm. An additional 520-nm long-pass filter (Schott, Mainz, Germany) was installed on the emission path. The fluorescence decays of BODIPY were measured with the emission polarizer set at 54.7° relative to the excitation polarizer. The time-dependent anisotropy decays were recorded for the emission polarizer set parallel and perpendicular relative to the excitation polarizer (7). For the magic-angle experiments, 30,000 counts were collected in the peak channel. In the depolarization experiments, the number of counts in the difference curve was 100,000. A minimum of three measurements was performed on at least two independent samples for each fraction of labeled actin. The absorbance at 505 nm was $<$0.08 to avoid reabsorption. Data were collected at 277 and 293 K; water condensation was avoided by purging cuvette surfaces with nitrogen.

Computer facilities

BD simulations were used to describe DDEM between fluorescent groups in F-actin. For the simulations and fitting of the GA, a Suse 9.2 Linux cluster of 6 AMD Sempron 3000, equipped with 2 GB of 400 MHz DDR memory was used. A 100 Mbit Ethernet was used for networking in the configuration of a star topology. Briefly, the simulations were performed in a local area multicomputer environment as described previously (12), using the parameters T_z,

θ, and T_{xy} to define the geometry of a regular protein polymer (Fig. 1). The distribution of donor-labeled subunits within the polymer is considered to be random, and their concentration corresponds to the mole fraction of labeled monomers in the experiment. For each donor, the BD simulation generates a reorientational trajectory, using a first-rank Maier-Saupe potential (12). The probabilities of DDEM between an initially excited donor and its neighbors were calculated within a cutoff distance of nine neighbors on each side. Based on this, the MC simulation of DDEM was performed by choosing a random moment of time when energy hopping occurs, and then choosing a random neighbor to which the energy migrates at the particular time-moment chosen. To calculate the average time-dependent fluorescence anisotropy, the procedure was repeated ~100,000 times. The MC simulation program was written in C++, using MPI libraries to accelerate computation time by parallel computations.

The depolarization data obtained for the most diluted sample (0.1%), i.e., in the absence of DDEM, was fitted by the Levenberg-Marquardt algorithm (L-MA) by simulations performed on a single donor. From this, the first-rank Maier-Saupe potential was determined, which was needed for global fitting of the samples containing larger fractions of the fluorophore-labeled actin (12.25, 24.5, and 49%) where the influence of DDEM on $r(t)$ is substantial. For the global fitting, the PIKAIA (17) variant of the GA written in Fortran 77, was used (see http://www.hao.ucar.edu/modeling/pikaia/pikaia.php). In the GA-analyses, 100–300 generations were used and repeated several times (5–10) for every data set, when using a random number as the initial seed. To speed up the procedure, the BD trajectories were calculated and stored in a random access memory. The fitting procedure was performed in two stages; first 180,000 BD trajectories were used and then 486,000 with more limited box constrains on the parameter space. Approximately 6 h and 16 h of computational time were needed for 180,000 and 486,000 number of trajectories, respectively.

THEORETICAL BACKGROUND

The genetic algorithm

Genetic algorithms (GA) are computational methods, which are inspired by the principal ideas of biological evolution (18), and used to construct numerical optimization techniques suitable for the analyses of an ill-behaved search space. Recently GA was implemented in fluorescence spectroscopy (19); here this approach is employed for the first time, to our knowledge, for analysis of fluorescent depolarization data collected by the TCSPC technique.

Briefly, the GA can be described by considering a model which depends on a set of N variables. The object is to find a set of variables within the N-dimensional box that minimizes the difference between the experimental data and the model prediction. The principle of operation to reach such a solution is outlined by the following: Start by generating a set of points (analogous to individuals) in the N-metric box as described by N-dimensional vectors (analogous to genomes) and then perform as follows:

1. Evaluate the model for every individual and calculate its fitness to data by means of the χ^2-measure, where fitness is defined by the reciprocal of χ^2. Here an individual refers to a specific parameter vector.
2. Select pairs of individuals from the current population to be parents, in proportion to their fitness.
3. Breed the two parameter vectors selected in step 2 into two new offspring, by means of crossover and mutation operations. Breeding is a procedure by which two new parameter vectors are created from the previous ones. Crossover refers to a deterministic procedure used to create new pairs of parameter vectors from the previous vectors. To avoid crossover parameters restricting the search to a subspace of the N-dimensional box, mutations are introduced.
4. Repeat steps 2 and 3 until the number of offspring equals the number of individuals.
5. Replace the old population with the new, which then becomes the next generation.
6. Repeat steps 1–5 until the fitness of one of the individuals becomes equal to a predefined value, or until a defined number of populations is reached.

As a result of the above procedure, the algorithm searches the genome for which the fitness, or reciprocal of χ^2, is maximized. For a detailed description of the genetic algorithm see Charbonneau (17) and visit the web sites (http://www.hao.ucar.edu/public/models/pikaia/breeding.html, and http://www.hao.ucar.edu/public/models/pikaia/pikaia.html).

Energy migration in many-donor systems

A theoretical treatment of DDEM within ensembles of donors as in the case of F-actin is complicated by the reversible energy transport occurring between numerous of these donors. The rate of energy migration is determined by rates of reorientation, as well as the spatial and orientational distributions of the donors. The DDEM process can be monitored by fluorescence depolarization experiments, which enable the calculation of the fluorescence anisotropy, $r(t)$. There is no analytical theory, however, that relates $r(t)$ to the above mentioned properties. Fortunately, these properties can be considered by BD and MC simulations, as described previously (12). To account for the local reorientations of the donor bound to a protein, BD simulations were implemented using a Maier-Saupe potential to model the molecular order. The potential was determined by fitting the BD simulations to the orientation correlation function of donors, which were studied in the absence of energy migration. To mimic $r(t)$ for a regular protein aggregate (see Fig. 1) by MC simulations, 401 subunits (= protein monomers) were considered and randomly labeled with a fluorophore at a fraction of f. The energy migration was accounted for within a cutoff distance of nine neighbors from each side from the initially excited fluorophore.

In the MC simulation, the spatial positions of all the donors and then all the neighbors within the cutoff distance were first defined. The BD trajectories are calculated over a long period of time, referred to T_∞. Then the total migration rate is calculated from

$$\Omega(t) = \sum_{j=-n}^{n} \omega_{0j}(t), \quad (1)$$

where $\omega_{0j}(t)$ is the rate of energy migration from the 0^{th} to the j^{th} donor, which is given by

$$\omega_{0j}(t) = \frac{3\kappa_{0j}^2(t)}{2\tau}\left(\frac{R_0}{R_{0j}}\right)^6. \quad (2)$$

Here τ, R_0, R_{0j}, and κ_{0j}^2 denote the donor fluorescence lifetime, the Förster radius, the distance between the 0^{th} to the j^{th} donor, and the square of the angular part of the dipole-dipole coupling, respectively. The explicit expression for the latter reads

$$\kappa_{0j}^2(t) = (\hat{\mu}_0(t)\cdot\hat{\mu}_j(t) - 3\{\hat{\mu}_0(t)\cdot\hat{R}_{0j}\}\{\hat{\mu}_j(t)\cdot\hat{R}_{0j}\})^2, \quad (3)$$

where $\hat{\mu}_k$ and $\hat{R}_{0j}$ are the unit vectors of the electronic transition dipoles and the distance vector between the centers of mass of the 0^{th} and j^{th} donor, respectively.

The coordinates of $\hat{\mu}_j$ with respect to the aggregate fixed frame are given by $\hat{\mu}_j(t) = \vec{A}_{\mu_j}(t) - \vec{O}(T_{xy}, T_z, \theta, j)$. Here $\vec{A}_{\mu_j}(t)$ denotes the vector directed from the origin of (X_A, Y_A, Z_A) to the point described by $\hat{\mu}_j$, and $\vec{O}(T_{xy}, T_z, \theta, j)$ describes the position of the center of mass of the j^{th} donor (see Fig. 1).

In the simulations, the energy of an initially excited donor migrates from one donor to another in a sequence of migration steps. The time elapsed between the excitation jumps is $t_{EM,i} = t_i - t_{i-1}$, where t_i and t_{i-1} denote the times of consecutive jumps. To simulate every event of energy migration, the following two questions need to be repeatedly answered:

1. When does an energy migration event take place?
2. Where does the excitation energy migrate?

The first question is to determine how long the excitation remains on the excited donor before the energy migration process takes place. The probability of the energy migration event at each moment is defined by total migration rate, $\Omega(t)$. To account for the time-dependence of $\Omega(t)$, the simulation time is divided into the time intervals Δt. These intervals are shorter than the characteristic time for the variation of $\Omega(t)$, which is caused by reorienting motions of the donors. For each interval Δt, the energy migration event is a random value which is distributed exponentially with a characteristic time $1/\Omega(t)$ according to

$$\tau_{EM} = -\frac{1}{\Omega(t)}\ln\eta, \quad (4)$$

where $\eta \in (0,1]$ is a uniformly distributed random number.

Values of $\tau_{EM} > \Delta t$ mean that the energy did not migrate within the current time step, whereby one Δt-step forward is taken. This involves the calculation of a new value of $\Omega(t)$, as well as the time, τ_{EM}. On the other hand, if $\tau_{EM} < \Delta t$, the energy migration takes place within the current time step. This procedure is terminated and the time of energy migration is determined to be $t_{EM,i} = n \times \Delta t + \tau_{EM}$. Here n denotes the number of steps of the procedure during which energy did not take place, and τ_{EM} is the random time generated in the last step.

Knowledge of the time of the next energy migration event at t_i raises the second question of where the energy migrates, i.e., to which D group among the labeled proteins. This is implemented in the MC simulation by making use of the probabilities of energy migration, which are given by

$$P_j(t_i) = \frac{\omega_{0j}(t_i)}{\Omega(t_i)}. \quad (5)$$

Here $\omega_{0j}(t_i)$ refers to energy migration rate the j^{th} fluorophore within the cutoff distance.

The time-dependent fluorescence anisotropy is calculated for the times $t \le T_\infty$. The procedure is repeated several times and forms the final ensemble average:

$$r(t) = r_0\langle\sum_j p_j(t)P_2(\hat{\mu}_0(0)\cdot\hat{\mu}_j(t))\rangle. \quad (6)$$

In Eq. 6, the subscript j runs over all donors, e.g., from -200 to $+200$, depending on the examined aggregate. When the j^{th} donor is excited, the probability, $p_j(t)$, is set equal to 1; if not, it is equal to 0. The expression $P_2(\hat{\mu}_0(0)\cdot\hat{\mu}_j(t))$ denotes the second Legendre polynomial.

The procedures above account for the local anisotropic motions of the donors groups, i.e., the energy migration under dynamic conditions.

RESULTS AND DISCUSSION

Polymerization characteristics of BODIPY-labeled actin

The penultimate amino-acid residue at the actin carboxyterminal C374 is widely used to generate pyrene-actin for polymerization studies where the increase in pyrene fluorescence upon incorporation of the conjugate in F-actin is recorded. Here, BODIPY was coupled to F-actin under similar conditions as used for pyrene-actin. After depolymerization, SDS-PAGE analyses demonstrated that the labeled actin was homogeneous and comigrates with nonderivatized actin (see Fig. 2). Comparison of BODIPY-actin with nonlabeled actin using MALDI-TOF after excision and in-gel digestion with trypsin, revealed the presence of a peptide identified as Q_{360}EYDESGPSIVHRKCF_{375} in the labeled actin, which was absent in the nonlabeled material (data not shown). This was interpreted as due to interference of the BODIPY group with trypsin cleavage at R372 and K373, and strongly pointed to C374 as the labeled residue.

Since the BODIPY-actin was intended to evaluate a new methodology for structural analyses of noncovalent protein polymers, it was important to investigate the polymer-forming properties of the labeled actin. This revealed that the fluorescence signal of BODIPY-actin changed dramatically upon polymerization in proportion to the fraction of labeled actin molecules present in the polymerizing sample (Fig. 2 *A*). Furthermore, addition of 2% pyrene-labeled actin to samples containing BODIPY-actin and recording the change in pyrene-fluorescence upon polymerization showed that the BODIPY-actin had no influence on the polymerization characteristics of the actin (Fig. 2 *B*). It was also observed

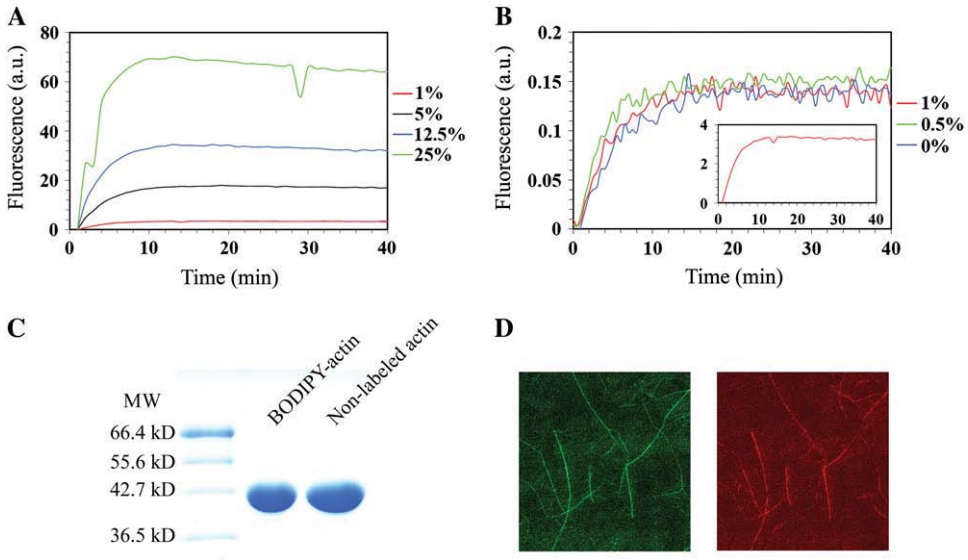

FIGURE 2 Polymerization and fluorescence properties of BODIPY-labeled β/γ-actin. (*A*) The increase in fluorescence upon polymerization of 8 μM β/γ-actin containing the fractions of fluorophore-labeled protein as indicated was recorded at 538 nm using an excitation wavelength of 485 nm (BODIPY fluorescence). (*B*) Pyrene fluorescence (excitation 365 nm, emission 410 nm) upon polymerization of 4 μM β/γ-actin containing 2% pyrene-actin and BODIPY-actin as indicated. (*Inset*) Recording of BODIPY fluorescence from the sample containing 1% of the actin labeled with BODIPY (*A*). Note that the BODIPY labeling does not influence the polymerization kinetics, and that the increase in relative fluorescence after polymerization reaches significantly higher values compared to pyrene-actin (see *A* and *B*). Panel *C* demonstrates the homogeneity of the labeled actin as seen by SDS-PAGE of 7.2 μg of labeled and 6.8 μg of nonlabeled protein, and panel *D* illustrates the visualization of BODIPY-labeled F-actin by fluorescence microscopy; (*left*) BODIPY-fluorescence (FITC filter) and (*right*) rhodamine-fluorescence due to double-staining with TRITC-phalloidin. β/γ-Actin at a concentration of 12 μM and consisting of 49% BODIPY-labeled actin was polymerized at room temperature and pipetted onto poly-L-lysine-coated coverslips followed by addition of 0.1 μM TRITC-phalloidin.

that the signal derived from BODIPY-actin was ~25-times stronger than the one from pyrene-actin (see *inset* in Fig. 2 *B*). This suggests that with BODIPY-actin, polymerization studies can be performed with much less modified actin than when using pyrene-actin as signaling actin-conjugate, making BODIPY-actin especially attractive for kinetic studies of samples containing low amounts of the protein. Another feature of BODIPY is that its fluorescence is readily visualized through FITC filters by standard fluorescence microscopy (Fig. 2 *D*). The labeling of the BODIPY-actin containing filaments with TRITC-phalloidin further demonstrated that polymerization of BODIPY-actin results in ordinary F-actin.

Fluorescence depolarization of BODIPY-labeled F-actin

Having established uncompromised polymer-forming properties for BODIPY-actin, we proceeded with the DDEM studies. BODIPY is ideal for DDEM experiments, since its spectral and photophysical properties remain quite invariant to the physicochemical nature of the environment (20,21). Fluorescence depolarization was recorded from the F-actin samples, and their anisotropy decays were calculated (see Fig. 3).

The $r(t)$-decays obtained for the most diluted sample ($f = 0.1\%$) demonstrated a fast initial decrease followed by a constant level after ~2 ns, suggesting fast local reorienting motions of the BODIPY group followed by a highly restricted orientation (see Fig. 3). The local rotational correlation times were 170 and 180 ps at 277 and 293 K, respectively, and the corresponding second-rank order parameters were $S \cong 0.93$ and 0.91. The plateau value shows that energy migration within the filaments as well as their overall reorientation is negligible on the timescale of the fluorescence. BD simulations were fitted to these data using the Levenberg-Marquardt algorithm to determine the Maier-Saupe potentials, which later were used for analyzing the depolarization data obtained in presence of DDEM (see Table 1). As indicated by the statistical χ^2-parameter, the fitting was good. The local motions and order of the BODIPY group were also determined for BODIPY-labeled G-actin. In contrast to F-actin, the $r(t)$-decays showed no residual anisotropy, which is compatible with an overall rotation tumbling of the protein on the timescale of fluorescence (see Fig. 3). This was accounted for in the determination of the local average rotational correlation time and order parameter of G-actin, which were 600 ps and 250 ps, and 0.88 and 0.86, respectively, at the two temperatures. Thus the local mobility of the BODIPY group in G-actin is somewhat slower and displays a slightly lower order, S, in comparison to F-actin, which suggests a different structural environment for C374 in the two states of the actin.

For F-actin, containing larger fractions of BODIPY-actin, the $r(t)$-decays became faster (see Fig. 3), with an increasing probability of DDEM as a result of the increasing mole fraction f. Even at $f = 1\%$, a substantial decay below the plateau value was observed (data not shown), which is explained by the onset of DDEM.

DDEM analysis based on the genetic algorithm

The analyses of the depolarization data obtained in the presence of DDEM make use of the Maier-Saupe potentials previously determined for generating the motional trajectories. These trajectories describe the local reorienting motions

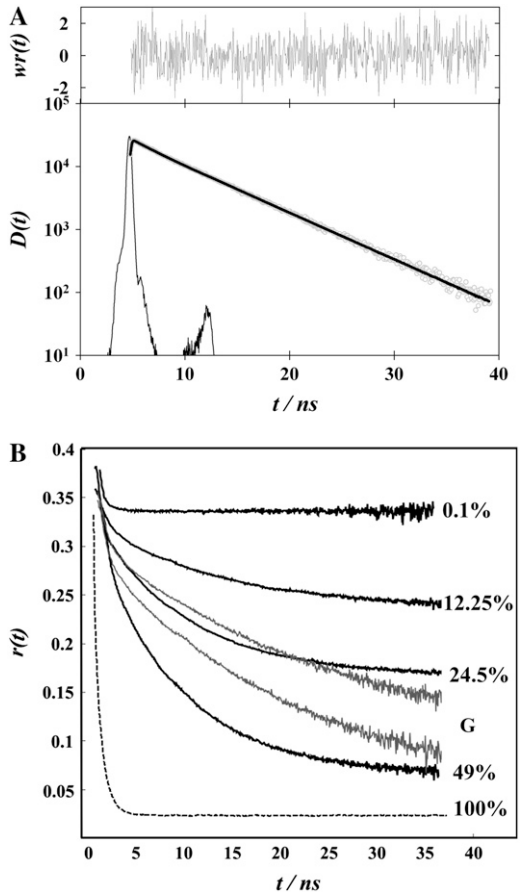

FIGURE 3 Fluorescence depolarization data obtained from the BODIPY-labeled F-actin. (*Top panel*) The results from the sample containing 0.1% BODIPY-labeled protein, showing the difference curve, $D(t)$. The experimental response function is shown below the $D(t)$ curve. The quality of a best-fit of the Maier-Saupe potential to $D(t)$ is illustrated by the weighted residuals, $wr(t)$. (*Lower panel*) The time-dependent fluorescence anisotropy, $r(t)$, calculated from the depolarization data obtained for F-actin containing different mole fractions of BODIPY-labeled actin at 277 K. The dashed curve was simulated using the parameters obtained in the global analyses and assuming 100% labeling of the actin. The $r(t)$-decays curves in shading were obtained for G-actin at 277 (*upper*) and 293 K (*lower*).

of the transition dipole of the BODIPY group in an actin monomer. The local reorienting motions, as well as the DDEM progress contribute to the fluorescence depolarization in a complex manner. Moreover, the rate of DDEM depends on the particular orientational distribution of the donors with respect to the actin monomers, the mutual orientation of the actin subunits in F-actin and their probability of being labeled. Five parameters account for these contributions (see Fig. 1); the two angles α_{DC} and β_{DC}, which specify the orientational distribution of BODIPY, and θ, T_{xy}, and T_z, which define the mutual localization of the next neighbors in F-actin. The GA was used to analyze the data and the typical convergence of the fitting is illustrated in Fig. 4, where the fitness of the best individual from every generation is plotted as a function of the number of generations. The optimization shows a stepwise manner of improvement, which is to be expected for an evolutionary algorithm. Repeating the minimization several times ensures that the global minimum is reached. For scanning the parameter space, the initial analyses used 180,000 trajectories and a wide range of parameter constraints, i.e., $-180° \le \alpha_{DC} \le 180°$; $0° \le \beta_{DC} \le 180°$; $-180° \le \theta \le -120°$; $8 \le T_{xy} \le 22$ Å; and $22 \le T_z \le 33$ Å. Values of θ, T_{xy}, and T_z were obtained for two sets of (α_{DC}, β_{DC}) angles (see Table 2). A detailed analysis was performed using 486,000 trajectories and the parameters obtained are presented in Table 2 and Fig. 5. The standard deviation was calculated from the results based on using different seeds for the random number generator. Note that the parameters belong to two categories, namely T_z and θ, which are independent of the donor position, and α_{DC}, β_{DC}, T_{xy}, which depend on its position.

TABLE 1 The depolarization data obtained for 0.1 mol % BODIPY-labeled F-actin after fitting to the Maier-Saupe potential, $U(\theta) = U_0\cos\theta$ (here, θ denotes the angle between the transition dipole moment and the C_∞-symmetry axis of the potential)

T/K	U (units of kT)	Diffusion constant/ns^{-1}	χ^2
277	66.40 ± 0.31	1.12 ± 0.04	1.085 ± 0.004
293	57.92 ± 0.73	1.30 ± 0.11	1.083 ± 0.005

A visualization of the results obtained from the GA analysis is displayed in Fig. 5, where χ^2 is plotted versus the α_{DC} and β_{DC} (see Fig. 5 *A*). The projected values of (α_{DC}, β_{DC}), (θ, α_{DC}), and (T_{xy}, T_z) for the χ^2-range of $1 \le \chi^2 \le 1.32$ are shown in Fig. 5, panels *B–D*, respectively. An increasing scatter of the data points was observed upon increasing the χ^2-values. For the presented parameters, the maximum spread is α_{DC} (±5.4°), β_{DC} (±2.1°), θ (±5.7°), T_{xy}(±0.5 Å), and T_z (±0.8 Å). Knowledge of the β_{DC} angle allows the prediction of experimental data from a sample containing 100% labeled protein. From the $r(t)$-decay (see Fig. 3) a plateau value of $r_\infty = 0.026$ was obtained. A limiting value is expected, because efficient energy migration among the BODIPY groups creates a uniaxial distribution of emitting dipoles about the C_∞-axis. This limiting anisotropy can also be calculated from $r_\infty = r_0 S^2\{P_2(\beta_{DC})\}^2$. Using the plateau value $r_0S^2 = 0.335$ obtained for $f = 0.1\%$ and $\beta_{DC} = 66.9°$ one obtains $r_\infty = 0.025$, which agrees with the value obtained from the simulations. Thus, the apparent plateau values obtained for the samples labeled to 24.5 and 49% do not correspond to a complete averaging about the C_∞-axis.

At steady state, F-actin is in a dynamic state with net growth at the fast polymerizing (+) end, and net dissociation of actin subunits from the slow polymerizing (−) end. Consequently, a small but finite monomer concentration is present in any filament population. A high monomer fraction (γ_G), can influence the resulting steady-state and time-resolved anisotropy $\{r(t)\}$ of the samples studied. This influence was eliminated by accounting for the anisotropy of

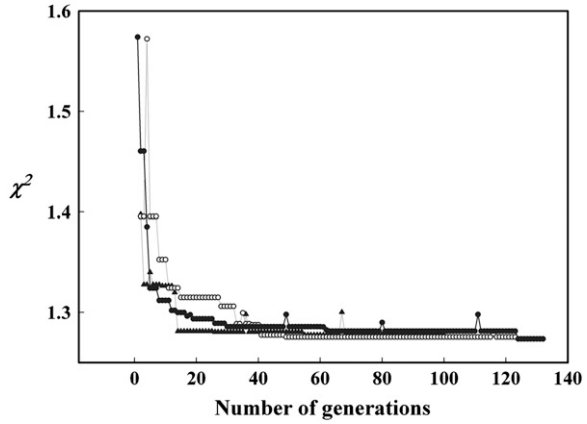

FIGURE 4 The convergent behavior of the GA for a global fitting of all data on F-actin obtained at 277 K, with 486,000 BD trajectories and a population size of 30 individuals. The statistical test of the best fit (χ^2) is plotted against the number of generations. Three independent fittings of the data are illustrated for three different initial seeds subjected to the random number generator.

the G-actin monomer $\{r_G(t)\}$ according to: $r(t) = (1 - \gamma_G)r_{sim}(t) + \gamma_G r_G(t)$, where $r_G(t)$ was constructed by fitting the time-resolved data of G-actin to a sum of exponential functions. The correction anisotropies were: $r_G(t, 277\ K) = 0.06\exp(-t/0.59) + 0.20\exp(-t/18.9) + 0.11$ and $r_G(t, 293\ K) = 0.06\exp(-t/0.72) + 0.24\exp(-t/17.8) + 0.05$, which together with the above equation results in a contribution of γ_G of $<2\%$.

DDEM results as compared to previously published data

The method tested here on filamentous actin enables prediction of the distribution of a repeating position for the center of mass of the donor molecule without any quantitative preliminary information of the polymer; the only requirement is that the structure is regular. The structural parameters T_z and θ are compatible with published data (see Table 2). For T_{xy}, which denotes the distance between the C_∞-axis and the center of mass of the fluorescent group attached to C374, there is, on the other hand, a discrepancy between the determination made here and reported values. The latter vary between 13.7 and 35 Å in different fluorescence studies (22–24), and x-ray crystallography in combination with fiber diffraction data (resolution ≈8 Å) places the C_α atom of C374 at a distance of 25–26 Å from the C_∞ axis (25). In striking contrast, $T_{xy} = 10.9 \pm 0.1$ Å at 277 K, and 10.6 ± 0.5 Å at 293 K in this study.

For several reasons the lower value of T_{xy} determined here appears to be a better estimate. Unlike previous analyses based on fluorescence studies and the crystallographic model of F-actin (13,26), the values T_z and θ were treated as floating parameters in this study. Previously it was assumed that $\langle\kappa^2\rangle = 2/3$ (14,22–24), while here the time-dependence was accounted for by BD simulations. This analysis also includes energy migration between nine neighbors on each side of the initially excited fluorophore compared to two used by Moens and dos Remedios (14) and only one by Taylor et al. (24). One can estimate the number of neighbors needed, from Miki et al. (27) according to

$$r_n = \sqrt{2T_{xy}^2(1 - \cos(166^\circ n) + (T_z n)^2)}. \quad (7)$$

Here n denotes the n^{th} neighbor counted from the initially excited molecule. The work in the literature (20,21) fulfills this criterion, while that in Moens and dos Remedios (22) does not. In this study, $R_0 = 57$ Å (20) and the distance to the fourth neighbor is $1.78R_0$, representing the minimum number of neighbors needed. Since the rate of energy migration depends on the molecular orientation, it is necessary to account for more than four neighbors, and for calculating the rate of energy migration, $\omega_{0j}(\kappa^2(t))$ (see Eq. 2), the number needed is bigger than the estimated value. Furthermore, for samples with lower fractions of labeled molecules, the energy migration/transfer to more distant monomers becomes important, but in none of the above cited studies was this influence, $\kappa^2(t)$, considered.

The significant difference found between the T_{xy}-value ($= 10.6 \pm 0.5$ Å) obtained here and the 25–26 Å reported in Holmes et al. (25) cannot be due to the linker length between the fluorescent group and the S-atom of C374, which is ≤7 Å. The orientation of the BODIPY group can be determined

TABLE 2 Three independent determinations at two different temperatures of the five structural parameters defining the actin polymer (see Fig. 1); the fraction of free G-actin γ_G was assumed to be zero or treated as a floating parameter in the analyses

F-actin	γ_G (%)	α_{DC} (°)	β_{DC} (°)	θ(°)	T_{xy} (Å)	T_z (Å)	χ^2
277 K	0	179.7 ± 0.2	66.9 ± 0.1	−160.4 ± 0.3	10.9 ± 0.0	26.4 ± 0.0	1.27 ± 0.00
277 K	0	169.9 ± 5.4	64.7 ± 5.4	−162.8 ± 2.2	10.8 ± 0.0	25.8 ± 0.3	1.28 ± 0.00
277 K	1.6 ± 0.1	164.5 ± 1.4	113.8 ± 0.5	−157.6 ± 1.3	11.1 ± 0.1	25.8 ± 0.2	1.29 ± 0.00
293 K	0	171.6 ± 3.8	115.7 ± 0.4	−155.6 ± 5.7	10.6 ± 0.5	26.2 ± 0.2	1.4 ± 0.01
293 K	0	177.6 ± 0.1	65.6 ± 0.0	−158.1 ± 1.5	10.2 ± 0.0	26.7 ± 0.1	1.42 ± 0.00
293 K	1.4 ± 0.1	165.7 ± 2.5	115.9 ± 2.1	−161.0 ± 1.7	10.7 ± 0.2	25.9 ± 0.8	1.41 ± 0.01
Data from literature				−166*	13.5†	27.5*	

486,000 trajectories were used in the data analyses.
*From Egelman et al. (13).
†From Moens et al. (14).

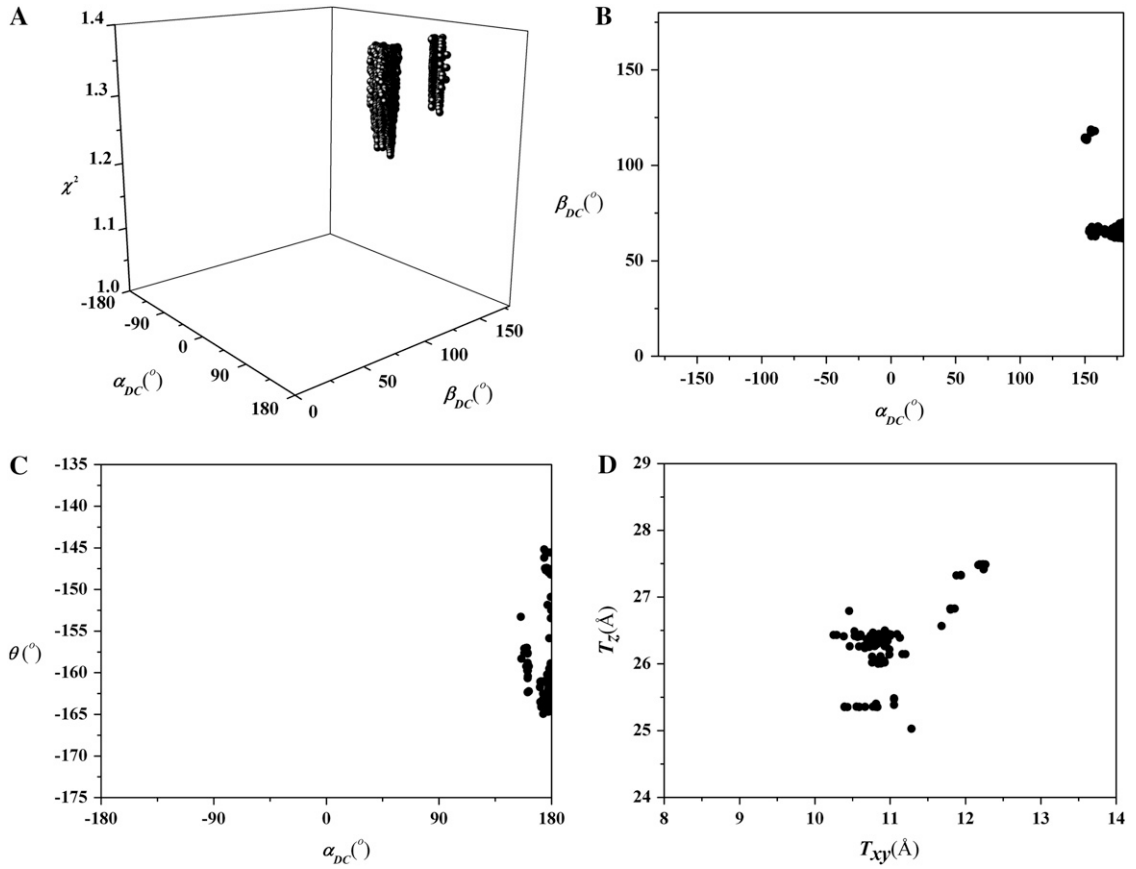

FIGURE 5 Results from the global GA analysis of the fluorescence depolarization data on F-actin at 277 K, using 486,000 trajectories in the BD simulations. Three different F-actin samples containing 12.25, 24.5, and 49 mol % of BODIPY-labeled F-actin were analyzed. T_{xy}, T_z, α_{DC}, and β_{DC} denote the structural parameters defined in Fig. 1. (*A*) The pairs of α_{DC} and β_{DC} corresponding to the global minima. (*B–D*) The projections of χ^2-values in the (α_{DC}, β_{DC})-, (α_{DC}, θ)-, and (T_{xy}, T_z)-planes for the range $1 \leq \chi^2 \leq 1.32$.

from the angles α_{DC} and β_{DC} (see Fig. 1). Two sets of (α_{DC}, β_{DC}) angles were obtained (see Table 2 and Fig. 5, *A* and *B*), which describe the possible directions of the effective symmetry axis, Z_D. The high value of the order parameter ($S \approx 0.9$) means that the electronic transition dipole of BODIPY (20) and its long axis is oriented nearly parallel to the Z_D axis. Using the (α_{DC}, β_{DC}) angles implies that the long axis of BODIPY is preferentially oriented parallel to the X_c axis. It then follows that the radial distance between the S-atom of C374 and the C_∞ axis is ~6.4 Å shorter than $T_{xy} = 10.9 \pm 0.01$ Å at 277 K, and 10.6 ± 0.5 Å at 293 K. Thus, this distance is between 5 and 11 Å, and the C374 residue therefore locates closer to the filament axes than previously anticipated. Either the protomers in the filament take a different orientation than previously modeled, or else changes in the G-actin structure upon polymerization accounts for this.

Comparison between the GA and the L-MA

General questions in the analyses of TCSPC data concern the development of realistic physical models, and the use of powerful methods for determining the relevant physical parameters. The parameters are considered to be linearly independent and they are varied until the best fit to the data is achieved. The fitting process is a question of optimization, for which several strategies exist. A standard gradient method, such as the L-MA, or a genetic algorithm can be used. In this work, data was initially analyzed using a standard L-MA, which proved to be sensitive to local minima. This means that by using different initial values, one may find different solutions. An obvious method might be to scan large combinations of the parameters using a grid, and then search for the minimum χ^2. Unfortunately, this method requires extensive computational time. In contrast, the more sophisticated method employing the GA is not sensitive to local minima and is therefore suitable for analyzing ill-behaved parameter spaces (17). In our experience, the time needed for the L-MA to find one (local) minimum is approximately the same as needed for the GA to find the global minimum.

CONCLUDING REMARKS

The GA was applied here in the analyses of structural parameters of F-actin, which involves the search for the best

fit with respect to five parameters. The results obtained are in agreement with the accepted view of the actin filament as a helical structure and refine the position of C374, which should encourage application of the GA in the analyses of TCSPC experiments. A versatile method was demonstrated with potential applicability to various noncovalent polymers, e.g., in structural studies of diseases related to amyloids (28,29) and prions (30,31). Other interesting examples are the cytolytic toxins (32,33), which are thought to create pores in membranes (34).

A logical continuation of these studies on F-actin is to label other positions in the protein, possibly after site-directed mutagenesis as described previously (e.g., (35,36)), to reach new insights about the filament subunit orientation.

We are grateful to Dr. Stanislav Kalinin and Dr. Pär Håkansson for help in developing a simulation program. We are also grateful to Dr. Lars Backman and to MSc Oleg Opanasyuk for valuable discussions.

This work was financially supported by the Kempe Foundations, the Carl Trygger Foundation, and the Swedish Research Council.

REFERENCES

1. Dickerson, R. E. 1964. X-Ray Analysis and Protein Structure. Academic Press, New York.
2. Blundell, T. L., and L. N. Johnson. 1976. Protein Crystallography. Academic Press, London.
3. Clore, G. M., and A. M. Gronenborn. 1993. Topics in Molecular and Structural Biology. The Macmillan Press, London.
4. Wütrich, K. 1986. NMR of Proteins and Nucleic Acids. Wiley, New York.
5. Van der Meer, B. W., G. Coker III, and S.-Y. S. Chen. 1994. Resonance Energy Transfer: Theory and Data. VCH Publishers, New York.
6. Valeur, B. 2002. Molecular Fluorescence. Principles and Applications. Wiley-VCH, Berlin.
7. Lakowicz, J. R. 1999. Principles of Fluorescence Spectroscopy. Kluwer Academic/Plenum, New York.
8. Vekshin, N. L. 1997. Energy Transfer in Macromolecules. SPIE Press, Bellingham, WA.
9. Kalinin, S., and L. B.-Å. Johansson. 2004. Utility and considerations of donor-donor energy migration as a fluorescence method for exploring protein structure-function. *J. Fluor.* 14:681–691.
10. Johansson, L. B.-Å., P. Edman, and P.-O. Westlund. 1996. Energy migration and rotational motion within bichromophoric molecules. II. A derivation of the fluorescence anisotropy. *J. Chem. Phys.* 105:10896–10904.
11. Håkansson, P., M. Isaksson, P.-O. Westlund, and L. B.-Å. Johansson. 2004. Extended Förster theory for determining intraprotein distances. 1. The K^2-dynamics and fluorophore reorientation. *J. Phys. Chem. B.* 108:17243–17250.
12. Marushchak, D., and L. B.-Å. Johansson. 2005. On the quantitative treatment of donor-donor energy migration in regularly aggregated proteins. *J. Fluoresc.* 15:797–804.
13. Egelman, E. 1985. The structure of F-actin. *J. Muscle Res. Cell Motil.* 6:129–151.
14. Moens, P. D. J., and C. G. dos Remedios. 1997. A conformational change in F-actin when myosin binds: fluorescence resonance energy transfer detects and increase in the radial coordinate of Cys^{374}. *Biochemistry.* 36:7353–7360.
15. Johansson, T., S. Grenklo, and R. Karlsson. 2004. Detection of binding partners to the profilin:actin complex by far Western and mass spectrometry analyses. *Anal. Biochem.* 335:228–234.
16. Reference deleted in proof.
17. Charbonneau, P. 1995. Genetic algorithms in astronomy and astrophysics. *Astrophys. J. Suppl. Ser.* 101:309–334.
18. Darwin, C. 1995. Origin of Species. Gramercy, New York.
19. Fisz, J. J., M. Buczkowski, M. P. Budzinski, and P. Kolenderski. 2005. Genetic algorithms optimization approach supported by the first-order derivative and Newton-Raphson methods: application to fluorescence spectroscopy. *Chem. Phys. Lett.* 407:8–12.
20. Karolin, J., L. B.-Å. Johansson, L. Strandberg, and T. Ny. 1994. Fluorescence and absorption spectroscopic properties of dipyrrometheneboron difluoride (BODIPY) derivatives in liquids, lipid membranes, and proteins. *J. Am. Chem. Soc.* 116:7801–7806.
21. Bergström, F., I. Mikhalyov, P. Hägglöf, R. Wortmann, T. Ny, and L. B.-Å. Johansson. 2002. Dimers of dipyrrometheneboron difluoride (BODIPY) with light spectroscopic applications in chemistry and biology. *J. Am. Chem. Soc.* 124:196–204.
22. Moens, P. D. J., and C. G. dos Remedios. 2001. Analysis of models of F-actin using fluorescence resonance energy transfer spectroscopy. *Results Probl. Cell Differ.* 32:59–77.
23. Kasprzak, A. A., R. Takashi, and M. F. Morales. 1988. Orientation of actin monomer in the F-actin filament: radial coordinate of glutamine-41 and effect of myosin subfragment 1 binding on the monomer orientation. *Biochemistry.* 27:4512–4522.
24. Taylor, D. L., J. Reidler, J. A. Spudich, and L. Stryer. 1981. Detection of actin assembly by fluorescence energy transfer. *J. Cell Biol.* 89:362–367.
25. Holmes, K. C., D. Popp, W. Gebhard, and W. Kasch. 1990. Atomic model of the actin filament. *Nature.* 347:44–49.
26. Popp, D., V. V. Lednev, and W. Jahn. 1987. Methods of preparing well-oriented sols of F-actin containing filaments suitable for x-ray diffraction. *J. Mol. Biol.* 224:65–76.
27. Miki, M., S. I. O'Donoghue, and C. G. dos Remedios. 1992. Structure of actin observed by fluorescence resonance energy transfer spectroscopy. *J. Muscle Res. Cell Motil.* 13:132–145.
28. Malisauskas, M., V. Zamotin, J. Jass, W. Noppe, C. M. Dobson, and L. A. Morozova-Roche. 2003. Amyloid protofilaments from the calcium-binding protein equine lysozyme: formation of ring and linear structures depends on pH and metal ion concentration. *J. Mol. Biol.* 330:879–890.
29. Malisauskas, M., J. Ostman, A. Darinskas, V. Zamotin, E. Liutkevicius, E. Lundgren, and L. A. Morozova-Roche. 2005. Does the cytotoxic effect of transient amyloid oligomers from common equine lysozyme in vitro imply innate amyloid toxicity? *J. Biol. Chem.* 280:6269–6275.
30. Aguzzi, A., and M. Polymenidou. 2004. Mammalian prion biology: one century of evolving concepts. *Cell.* 116:313–327.
31. Houston, F., W. Goldmann, A. Chong, M. Jeffrey, L. Gonzalez, J. Foster, D. Parnham, and N. Hunter. 2003. Prion diseases: BSE in sheep bred for resistance to infection. *Nature.* 423:498.
32. Stanley, P., V. Koronakis, and C. Hughes. 1998. Acylation of *Escherichia coli* hemolysin: a unique protein lipidation mechanism underlaying toxin function. *Microbiol. Mol. Biol. Rev.* 62:309–333.
33. Abrami, L., M. Fivaz, and F. G. van der Goot. 2000. Adventures of a pore-forming toxin at the target cell surface. *Trends Microbiol.* 8:168–172.
34. Wai, S. N., M. Westermark, J. Oscarsson, J. Jass, E. Maier, R. Benz, and B. E. Uhlin. 2003. Characterization of dominantly negative mutant ClyA cytotoxin proteins in *Escherichia coli*. *J. Bacteriol.* 185:5491–5499.
35. Schüler, H., E. Korenbaum, C. E. Schutt, U. Lindberg, and R. Karlsson. 1999. Mutational analysis of Ser^{14} and Asp^{157} in the nucleotide-binding site of β-actin. *Eur. J. Chem.* 265:210–220.
36. Schüler, H. R. Karlsson, and U. Lindberg. 2006. Purification of non-muscle actin. *In* Cell Biology, 3rd Ed. J. Celis, editor. Elsevier, San Diego, CA.
37. Chik, J. K., U. Lindberg, and C. E. Schutt. 1996. Structure of bovine β-actin-profilin complex with actin-bound ATP phosphates solvent-accessible. *In* Protein Data Bank. 1HLU.
38. Chik, J. K., U. Lindberg, and C. E. Schutt. 1996. The structure of an open state of β-actin at 2.65 Å resolution. *J. Mol. Biol.* 263:607–623.